Available online at www.sciencedirect.com
SCIENCE DIRECT
Journal of Catalysis 234 (2005) 219–229
JOURNAL OF CATALYSIS
www.elsevier.com/locate/jcat

NO_x adsorption over a wide temperature range on Na-ZSM-5 films

Indra Perdana [a,*,1], Derek Creaser [a], Olov Öhrman [b], Jonas Hedlund [b]

[a] *Department of Chemical Engineering and Environmental Science, Chalmers University of Technology, SE-412 96, Gothenburg, Sweden*
[b] *Div. of Chemical Technology, Luleå University of Technology, SE-971 87, Luleå, Sweden*

Received 16 March 2005; revised 30 May 2005; accepted 9 June 2005

Available online 21 July 2005

Abstract

NO_x adsorption over a wide temperature range (30–350 °C) on monolith supported Na-ZSM-5 films were studied with a gas flow reactor. The nature of the adsorbed species was further investigated by in situ infrared spectroscopy. Depending on the adsorption temperature, three different ranges of thermally stable species were observed on Na-ZSM-5 films. In addition to the role of cationic sites and residual hydroxyl groups in zeolite frameworks, it was found that the formation of nitric acid plays an important role in NO_2 adsorption. Nitrate species were formed during adsorption by two mechanisms. The nitrates formed via nitric acid and involving NO formation had lower thermal stability than those formed through an NO_2 disproportionation reaction.

Keywords: NO_x adsorption; Monolith; ZMS-5 films; Adsorption mechanisms

1. Introduction

Zeolites are alumina silicates with a well-defined crystalline structure with cavities and pores of molecular dimensions. Positively charged cations are often required in the structure to balance the charge. These cations are exchangeable and influence the catalytic and transport properties of the zeolite. These characteristics make zeolites promising materials for catalysis and separation applications. Among the different types of zeolites, the MFI type in particular (i.e., ZSM-5 and silicalite-1) is widely used and studied.

For separation applications, zeolite crystals may be intergrown to form a film on a porous support material, resulting in a zeolite membrane. The selective permeation of a certain component through zeolite membranes strongly depends on both the adsorption properties and mobility of the component in the zeolite. Zeolite powder samples are commonly used to study the adsorption of components on zeolites. However, a direct adsorption study using a zeolite film with crystal morphology similar to that of the membranes can lead to a better understanding of the adsorption and transport properties for a membrane. Recently, it was possible to coat monolithic and other structured support materials with binder-free zeolite films [1–3], and the films were catalytically active [2,3]. However, it has been found that the presence of defects in thick films could increase the effective diffusivity and eventually reduce catalyst selectivity [4,5].

NO_x adsorption on catalytic materials has been an important research topic for the development of transport and stationary exhaust after treatment systems. Investigations of NO_x adsorption on cation-exchanged zeolites have been reported in a number of publications. It has been found that NO is much more weakly adsorbed than NO_2 on several cation-exchanged zeolites [6,7] and requires a low temperature for storage [8,9]. To obtain storage of NO, oxidation to NO_2 is required [6,10,11]. Depending on the nature of the zeolite, various adsorbed NO_x species may exist. Infrared studies, mostly at near-ambient temperatures, show that in most cation-exchanged zeolites, surface nitrate species are formed after NO_x exposure, and the species are mainly located on the metal sites [7,11–14].

* Corresponding author. Fax: +46-31-7723035.
E-mail address: creaser@chemeng.chalmers.se (D. Creaser).
[1] On leave from Department of Chemical Engineering, Gadjah Mada University, Indonesia.

0021-9517/$ – see front matter
doi:10.1016/j.jcat.2005.06.007

However, there is no information now available concerning NO_x adsorption on the zeolite in the form of a film. The present work is devoted to a study of the adsorption of NO_x on an oriented Na-ZSM-5 film supported on a cordierite monolith. The presence of adsorbed NO_x species is studied by temperature-programmed desorption (TPD) and in situ DRIFT spectroscopy. In this report an adsorption mechanism is also proposed. The results from this work give valuable insights into NO_x adsorption and transport in Na-ZSM-5 films or membranes.

2. Experimental

2.1. Sample preparation

The Na-ZSM-5 film samples were prepared on cordierite monoliths. The monoliths consist of 188 channels in the cross section with a channel dimension of 1 × 1 mm. A detailed description of the sample preparation procedure has been reported elsewhere [2]. The monoliths were seeded with 60-nm silicalite-1 seeds [15,16] and hydrothermally treated repeatedly at atmospheric pressure at 75 °C for 48 h. The seeded monolith samples used in this work were hydrothermally treated 12 times in a synthesis solution with a molar composition of 3 TPAOH:25 SiO_2:0.25 Al_2O_3:1 Na_2O:1600 H_2O:100 EtOH. Between hydrothermal treatments the samples were rinsed with 0.1 M aqueous ammonia solution and treated with ultrasound for 10 min. After the last hydrothermal treatment the samples were rinsed in a 0.1 M aqueous ammonia solution for 4 days and treated with ultrasound for 1 h each day. To remove precipitated zeolite from the ends of the monoliths, the monoliths were polished on each side to a length of 75 mm.

A powder sample for in situ DRIFT spectroscopy measurements was prepared from a synthesis solution with the same composition as that used for film growth. The resulting ZSM-5 crystals were hydrothermally treated for 72 h at 100 °C, but without the support and silicalite-1 seeds [2]. To remove the template material, the monolith and powder samples were finally calcined at 550 °C for 6 h with a heating and cooling rate of 1.75 °C min^{-1}.

The samples were characterized by scanning electron microscopy (SEM) (Philips XL 30) and with nitrogen sorption (Micromeritics ASAP 2010). It was found that the surface area of the support is negligible compared with the total surface area of the sample [5]. Therefore, the zeolite loading was determined from gas sorption data (BET), with the surface area of ZSM-5 powder (415 m^2/g) as a reference [5,17]. The elemental content of the powder sample was determined by inductively coupled plasma atomic emission spectroscopy (ICP-AES).

2.2. Adsorption–desorption measurements

NO_2 adsorption measurements were performed in a gas-flow reactor. The reactor consisted of a horizontal quartz tube with a length of 880 mm and a diameter of 22 mm and was equipped with a circular electrical heating element on the outer surface of the tube. To regulate the gas temperature and measure the sample temperature, two thermocouples were placed in the reactor. The monolith sample was sealed in the quartz tube with glass wool to prevent the gas flow from bypassing the channels. The two thermocouples were inserted into channels near the center of the monolith and from the downstream end of the monolith. One thermocouple was inserted about 5 mm into the monolith, whereas the second thermocouple traversed the entire length of the monolith so that it protruded about 10 mm out of the upstream end. We minimized heat loss by enclosing the reactor with glass wool insulation. Before NO_2 adsorption, the sample was pretreated with 8% O_2 in argon at 500 °C for 15 min at a total flow rate of 3000 ml/min (STP). After the pretreatment, the sample was cooled to the adsorption temperature and equilibrated in an argon flow. For the adsorption, a gas mixture at a total flow rate of 2600 ml/min (STP) containing 600 ppm NO_2 in argon was prepared in a gas mixer (Environics 2000) consisting of several mass flow controllers. The temperature was regulated with a temperature controller (Eurotherm), with the use of the measurement from the thermocouple positioned 10 mm in front of the sample. After adsorption, the sample was flushed with only argon at the adsorption temperature. Finally, to release all of the adsorbed species, the sample was heated from the adsorption temperature to 550 °C with a temperature ramp of 20 °C/min in an argon atmosphere during TPD.

In some experiments, the sample was also exposed to NO in argon. The influence of NO on the adsorbed species was investigated at 350 °C. The sample was first equilibrated with 600 ppm NO_2 for 20 min. After establishment of equilibrium, the sample was flushed with argon for 5 min. Subsequently, at the same temperature, 600 ppm NO in argon was introduced at the inlet. In addition, the influence of NO was further studied by NO_2/NO co-adsorption experiments. During adsorption and desorption the outlet gas composition was analyzed online with a chemiluminesence detector (Ecophysics CLD 700 EL ht). The amount of adsorbed/desorbed NO_x was quantified from the area under corresponding concentration curves of adsorption, flushing, and TPD.

2.3. In situ DRIFT spectroscopy measurements

In situ DRIFT spectroscopy measurements were performed with a rapid scan method with a Bio Rad FTS6000 spectrometer. The zeolite powder was placed in a sample holder assembly in a Harrick Praying Mantis DRIFT cell. The gases were supplied by individual mass flow controllers with a total flow rate of 200 ml/min (STP). Before NO_2 ad-

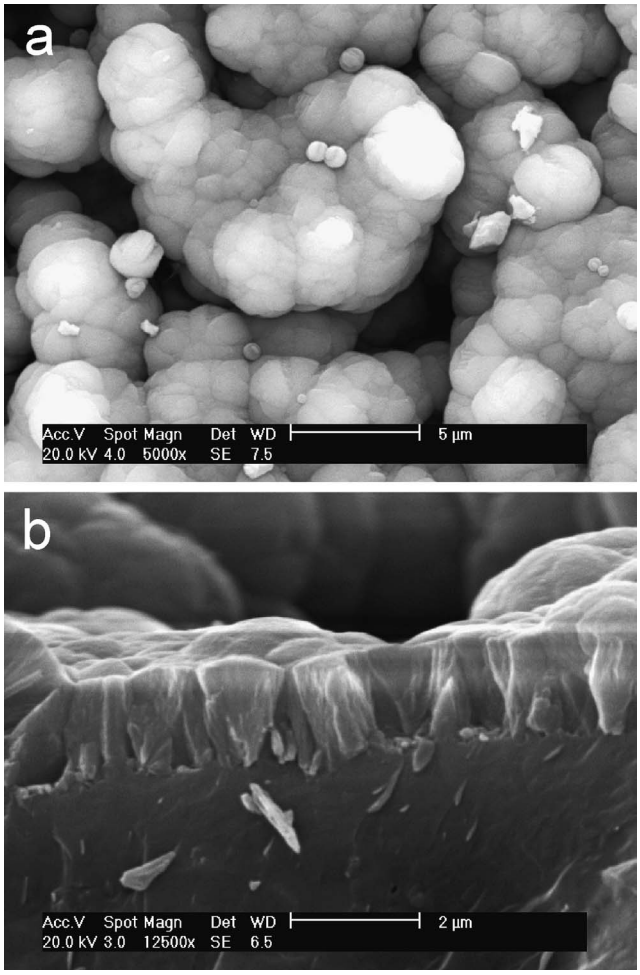

Fig. 1. (a) Top view of Na-ZSM5 film, (b) side view of Na-ZSM5 film.

sorption, the sample was pretreated with 8% O_2 in argon at 500 °C for 15 min. The sample was then cooled to adsorption temperature and equilibrated in an argon atmosphere. The adsorption experiment was performed by the introduction of 600 ppm NO_2 in argon. After the NO_2 adsorption, the sample was flushed with argon. To observe the influence of NO, the NO_2 equilibrated sample was then flushed with 600 ppm NO. Finally, to release the adsorbed species from the sample, the temperature was increased to 500 °C and was then kept constant for about 20 min. Each spectrum taken was the average of 100 scans with a resolution of 2 cm^{-1}.

3. Results and discussion

3.1. General sample characteristics

The seed crystals were homogeneously distributed over the entire support surface. Figs. 1a and b show top- and side-view SEM images of the prepared film. The polycrystalline film is composed of columnar crystals grown from seed crystals deposited on the monolith surface in the same way as reported before [2,4,5]. The film thickness is about 1.7 µm,

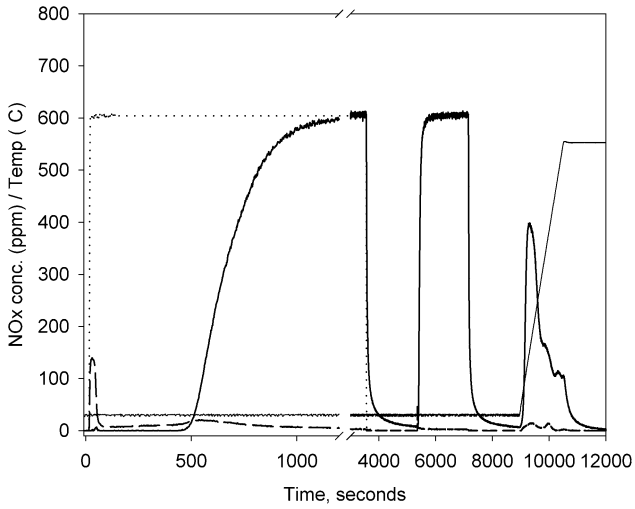

Fig. 2. Measured NO_x composition out of the reactor upon exposure to 600 ppm NO_2 for 60 min at 30 °C followed by a 30 min argon flush, 30 min NO_2 re-adsorption, 30 min argon flush at constant temperature and finally a temperature ramp of 20 °C/min (thick solid line, NO_2; dashed line, NO; dotted line, NO_2 from empty reactor; thin solid line, temperature).

as can be seen in Fig. 1b. The top view shows that the surface of the film is rough because of the porous surface of the cordierite [2,4,5]. Some crystal deposits originating from the bulk of the synthesis solution are also observed on top of the film surface, as observed and reported before [2]. In addition, some cracks and open grain boundaries were found in several parts of the film, in accordance with previous reports [2,4,5]. The zeolite loading was calculated from N_2 adsorption measurement data, and it was 0.14 g zeolite/g sample.

The Si/Al and Si/Na ratios of the ZSM-5 powder sample were determined from the elemental content measured by ICP-AES. The powder formed in a synthesis solution with the same composition as that for film preparation had an Si/Al ratio of 63.8 and an Al/Na ratio of 0.9. According to SEM measurement, the powder was found to consist of 1-µm rounded twin crystals [5].

It was reported [2] that 6–9-µm-thick films grown on the cordierite support had Si/Al ratios similar to that of a powder measured by energy dispersive X-ray (EDX) and ICP-AES, respectively. The powder and films were prepared with synthesis solutions of identical composition. However, because of interference from the cordierite support, direct analysis of the composition of the thinner film (1.7 µm) used in the present work by EDX was inconclusive. As a result, the incorporation of traces of cations from the cordierite either during the film synthesis or during calcination by solid-state ion exchange [2,5] cannot be ruled out.

3.2. NO_2 adsorption on films

The NO_x concentration in the reactor effluent during a transient NO_2 adsorption–desorption experiment with two NO_2 adsorptions at 30 °C is depicted in Fig. 2. The first adsorption is after pretreatment and the second (re-adsorption)

is after argon flushing following the first adsorption. During the first adsorption, a large uptake of NO_2 is observed, indicated by the long time needed to reach equilibrium (600 ppm NO_2 in effluent). In contrast, the NO_2 response is only a few seconds for an empty reactor (reactor without monolith sample) experiment. When the sample is exposed to NO_2 a peak in NO concentration is observed immediately, and the concentration of NO in the effluent remains low when the sample is equilibrated with NO_2. This observation indicates that NO_2 adsorption likely involves a fast surface reaction, resulting in simultaneous NO formation and NO desorption. As shown in Fig. 2, the adsorption at 30 °C proceeds with a very low concentration of NO and NO_2 present over about 8 min. This period is mainly dependent on the total adsorption capacity. Further adsorption time results in an increase in NO_2 concentration in the effluent because the NO_2 convective transport through the monolith exceeds the total flux of NO_2 transported into the zeolite film. Although the NO_2 concentration in the effluent steeply increases, the system does not reach equilibrium immediately. Furthermore, the adsorption still proceeds with the production of NO, resulting in a very low concentration of NO in the effluent.

Szanyi et al. reported that zeolites adsorb NO very weakly, even at room temperature [7]. As a result, most net NO produced because of NO_2 storage should leave the zeolite surface by desorption into the gas phase. The data in Fig. 2. in combination with the fact that zeolites adsorb mainly NO_2 and only a small amount of NO, show that the NO_2 storage at 30 °C resulting in NO formation accounts for only a small part of the total storage of NO_2. Furthermore, since a high concentration of NO is observed only in the beginning of NO_2 adsorption; this indicates that NO mainly forms when NO_2 is adsorbed on a strong site.

After equilibrium was reached, the sample was flushed with argon. Fig. 2 shows that mostly NO_2 is released during this treatment. The release is mainly from physisorbed species. However, because of a high mass transport resistance in the film at low temperature, the release occurs very slowly. Experiments with different film samples (0.8- and 1.9-μm-thick films), as we have reported elsewhere, showed that mass transport resistance influenced the rate of NO_2 adsorption. In contrast, a drop in NO_2 concentration was observed within a few seconds in an experiment with an empty reactor.

NO_2 re-adsorption after argon flushing gives a different concentration profile compared with the previous adsorption. Equilibrium is reached much faster during the re-adsorption. It seems that the re-adsorption successfully recovers the physisorbed species released during argon flushing. In contrast to the first adsorption, NO desorption is absent from the NO_2 re-adsorption. This suggests that the species resulting from NO formation are stable during flushing with argon and still occupy surface sites and that these species are adsorbed strongly. An argon flushing following the equilibration releases the physisorbed species again with the same effluent concentration profile as in the previous flushing.

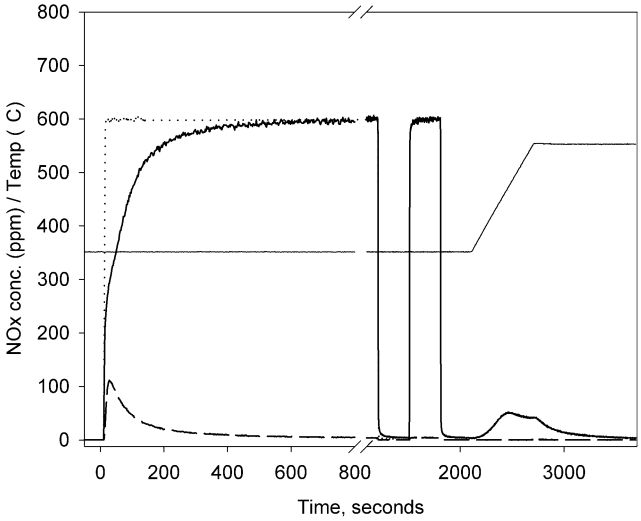

Fig. 3. Measured NO_x composition out of the reactor when the sample was exposed to 600 ppm NO_2 at 350 °C for 20 min followed by a 5 min argon flush and NO_2 re-adsorption for 5 min (thick solid line, NO_2; dashed line, NO; dotted line, NO_2 from empty reactor; thin solid line, temperature).

Similar adsorption phenomena arise from the adsorption at higher temperatures. Fig. 3 shows that NO_2 adsorption at 350 °C also occurs with simultaneous NO formation but reaches equilibrium more quickly than at 30 °C. The NO concentration in the effluent increases instantaneously once the sample is exposed to NO_2, resulting in a concentration peak. However, the NO concentration decreases slowly with additional adsorption time, resulting in a broad peak.

In comparison with the adsorption at 30 °C, the sample obviously has a lower storage capacity at 350 °C, since equilibrium is reached after a shorter time. As we reported elsewhere, adsorption and mass transport in the zeolite film are thermally activated, so that the rates of both adsorption and mass transport are faster at elevated temperatures. The smaller effect of mass transport resistance in the film at 350 °C is also indicated by the quicker responses of the gas concentrations during flushing and re-adsorption. The NO_2 gas concentration in the effluent reaches the feed concentration rapidly. The peak of NO from the adsorption at 350 °C is broader and has a lower maximum. The broader peak indicates that the time needed to saturate the adsorption sites, leading to NO formation, is longer probably due to the much lower NO_2 concentration in the film at the higher temperatures.

After NO_2 adsorption at both 30 °C (Fig. 2) and 350 °C (Fig. 3), it is predominately NO_2 that is desorbed during TPD. A small amount of NO was desorbed during TPD after adsorption at 30 °C (Fig. 2). It is probably mostly physisorbed NO released from NO_2 adsorption at low temperatures. However, at higher adsorption temperatures, for example 350 °C in Fig. 2, no desorption of NO was detected.

Since the quantity of NO_2 entering the reactor is known, the amount of adsorbed/desorbed NO_x can be quantified by

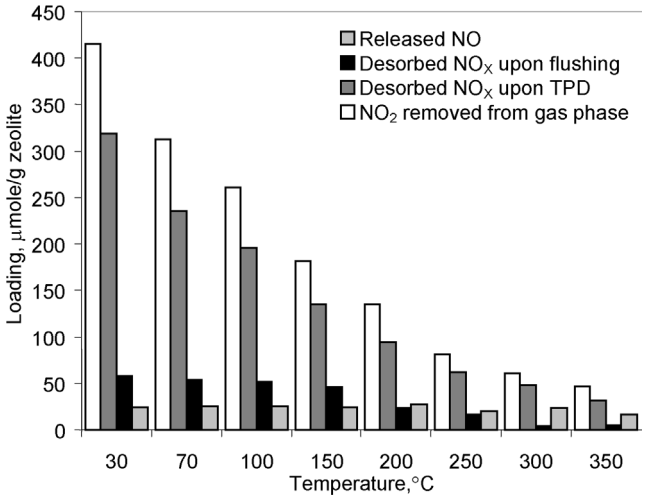

Fig. 4. The amount and distribution of adsorbed species at varying temperature after exposure to 600 ppm NO_2 with a total flow rate of 2600 ml/min (STP).

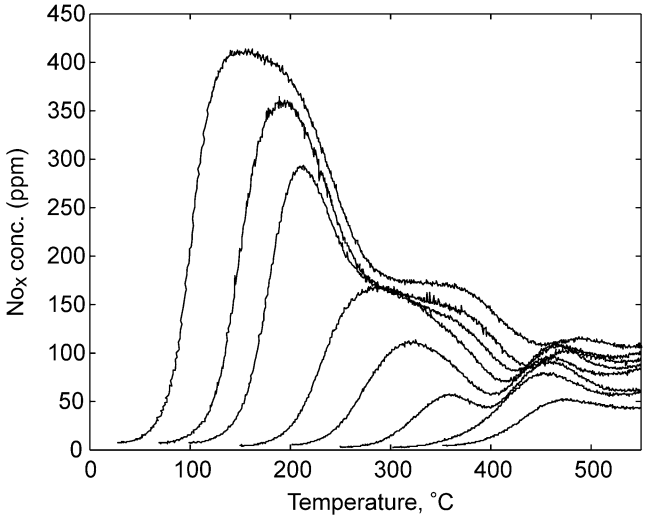

Fig. 5. NO_x concentration profiles during TPD after NO_2 equilibration and argon flushing at various temperatures.

integration of the area under the corresponding curves of adsorption, flushing, and TPD. The amounts of various adsorbed species after NO_2 adsorption at varying temperatures are listed in Fig. 4. The figure shows that the amount of NO formed and desorbed during NO_2 adsorption is almost constant over the entire investigated temperature range, indicating that NO formation is associated with NO_2 adsorption on strong sites. These sites will be saturated at all temperatures, resulting in a constant amount of NO formed. The amount of NO_x released during flushing decreases slightly in an adsorption temperature range of 30–150 °C. The release is significantly lower at 200 than at 150 °C and is insignificant above 250 °C.

The rate of desorption during flushing is dependent on the transport properties and the nature of the species at corresponding temperatures. Because of thermally activated diffusion in zeolites, less mass transport resistance is expected at high temperatures. Therefore, during low-temperature flushing, only a portion of the physisorbed species are detectable and may be removed. Part of the physisorbed species may still remain in the zeolite. On the other hand, at high temperatures it is more likely that all weakly adsorbed species are released during the flushing period and only strongly adsorbed species still remain on the surface, requiring higher temperatures for desorption.

The residual weakly adsorbed species, remaining in the interior of the zeolite after flushing, can easily be released as the temperature increases. It is expected that mostly these species are released at the beginning of TPD (see Figs. 2 and 5). It is thus more difficult to accurately determine the amount of chemisorbed species in the film from NO_2 adsorption at low temperatures by TPD.

Fig. 4 also indicates that at higher temperatures the storage resulting in NO formation seems to play a more important role in the NO_2 adsorption. The figure shows that NO is also formed during the adsorption at the highest investigated temperature and the amount changes little compared with that at low temperatures. This observation indicates that the NO formation might correspond to the formation of stable adsorbed species on strong adsorption sites. These species need higher temperatures for decomposition and desorption. Moreover, this is supported by the fact that in contrast to the adsorption at 30 °C, both NO_2 and NO immediately appear in the reactor effluent when the sample is exposed to NO_2 at 350 °C (see Fig. 3). At increasing temperature, NO_2 adsorption resulting in NO formation accounts for an increasing portion of the total NO_x storage.

The thermal stabilities of the adsorbed species over a wide adsorption temperature range are shown in Fig. 5. The concentration profiles are the results obtained from TPDs following equilibration at varying temperatures and flushing with argon. The results show that the adsorbed species can be classified into three types resulting in concentration maxima at low (100–200 °C), intermediate (250–350 °C), and high (400–500 °C) temperature. The first maximum is reached quickly and might correspond to physisorbed NO_2 and other weakly adsorbed species remaining in the interior of the zeolite after flushing. The second maximum is due to moderately thermally stable species and the third to nitrate species.

The influence of NO on the adsorbed species was further investigated at 350 °C by the introduction of NO after NO_2 equilibration and argon flushing. Fig. 6 shows that NO_2 immediately appears after introduction of NO. The concentration of NO_2 then decreases and levels out at an insignificant level as time increases, suggesting that the process has reached equilibrium. The release of NO_2 during NO exposure suggests that the reverse of the process that formed NO during NO_2 exposure occurs. Furthermore, since insignificant amounts of NO and NO_2 are physisorbed at 350 °C (see Figs. 3 and 5), the release of NO_2 upon exposure to NO is not due simply to an exchange of physisorbed NO_2 for NO.

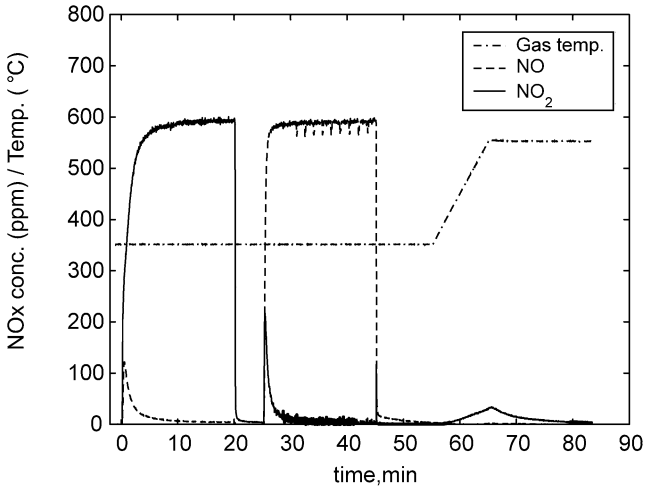

Fig. 6. Outlet NO_x concentration when the sample was exposed to 600 ppm NO_2 at 350 °C for 20 min followed by a 5 min flushing with argon, 20 min exposure to 600 ppm NO and finally a temperature ramp of 20 °C/min.

These observations thus indicate a reversible reaction involving NO_2 and NO occurs to form a strongly adsorbed species. This is in agreement with another report, which proposes a reversible reaction for nitrate species formation involving NO as a by-product but on Cu-ZSM-5 [5].

A TPD with a temperature ramp of 20 °C/min after 10 min of re-flushing in argon following 20 min of NO exposure results in an additional NO_2 release. As revealed in Fig. 6, the NO_2 concentration in the effluent is still increasing at 550 °C. However, mass balance calculations indicated that the remaining stored NO_x was desorbed when the maximum temperature was kept constant for about 15 min. Several repeated experiments have also been reproducible. The amount of stored NO_x was reduced by about 34% after the introduction of NO.

Fig. 7 shows concentration profiles in the reactor effluent during TPD after different treatments following equilibrium with the NO_2 feed at 350 °C. Without NO addition, as shown in Fig. 7a, TPD following NO_2 equilibration and argon flushing at 350 °C results in a maximum desorption rate at about 470 °C. However, the exposure to NO before the TPD removes the peak (see Fig. 7b). This result suggests that another kind of adsorbed species may be present that has a higher thermal stability than the adsorbed species formed that produced NO. In addition, the TPD following the NO introduction and flushing does not result in the appearance of NO. This observation suggests that the disappearance of the peak from TPD is not due to a competitive adsorption but mainly to a surface reduction. This further strengthens the evidence for a reversible reaction for NO_2 adsorption on strong sites.

As mentioned previously, bulk elemental analysis of the powder sample measured by ICP-AES shows an Al/Na ratio of 0.9. This result apparently suggests that the charge of all framework Al atoms might be balanced by Na cations. However, this bulk elemental analysis result does not necessarily indicate the status of cations throughout as-synthesized ZSM-5 crystals or films. Both Brønsted OH and excess Na in the form of Na_2O might also be present in the sample.

3.3. *In situ DRIFT spectroscopy results*

Fig. 8 shows that a feed of 600 ppm NO_2 in argon at 30 °C over a Na-ZSM-5 powder sample results in the appearance of an infrared band series. Accompanying the NO_2 adsorption, several intense peaks were observed in a wave number range of 1800 to 1200 cm^{-1}. On the other hand, in a higher wave number range (3800–2400 cm^{-1}), broad spectra were found. Flushing the NO_2-saturated sample with argon results in a slight intensity decrease for almost the whole spectrum. However, the peaks with bands at 1627 and 1601 cm^{-1} are completely removed upon argon flushing. These peaks probably correspond to physisorbed NO_2 [18,24]. As observed in the experiments with monolith samples, these species contribute to the gas-phase NO_x desorption during argon flushing. Additional time for argon flushing was found not to cause a significant change in the infrared spectra.

Also in Fig. 8, another peak with a large decrease in intensity after argon flushing is the peak with a band at 2135 cm^{-1}. This peak has been reported in several publications [14,18,22,24] as the stretching vibration of NO^+ on

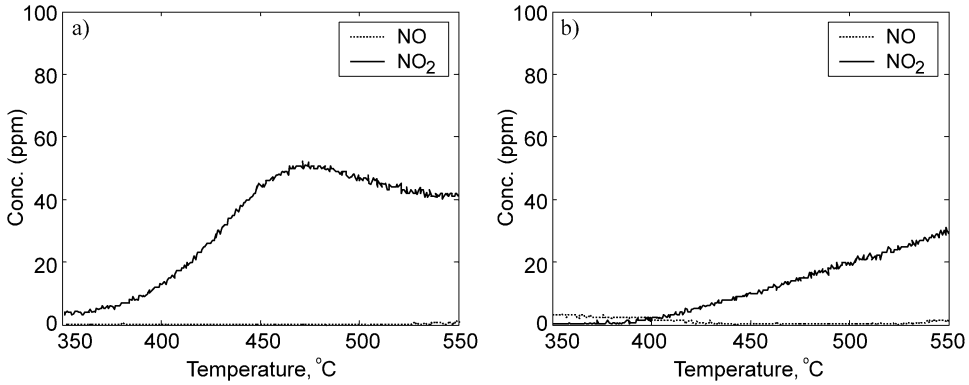

Fig. 7. NO_x concentration profiles from TPD after NO_2 equilibration and flushing in argon at 350 °C without subsequent NO exposure (a) and with subsequent NO exposure (b).

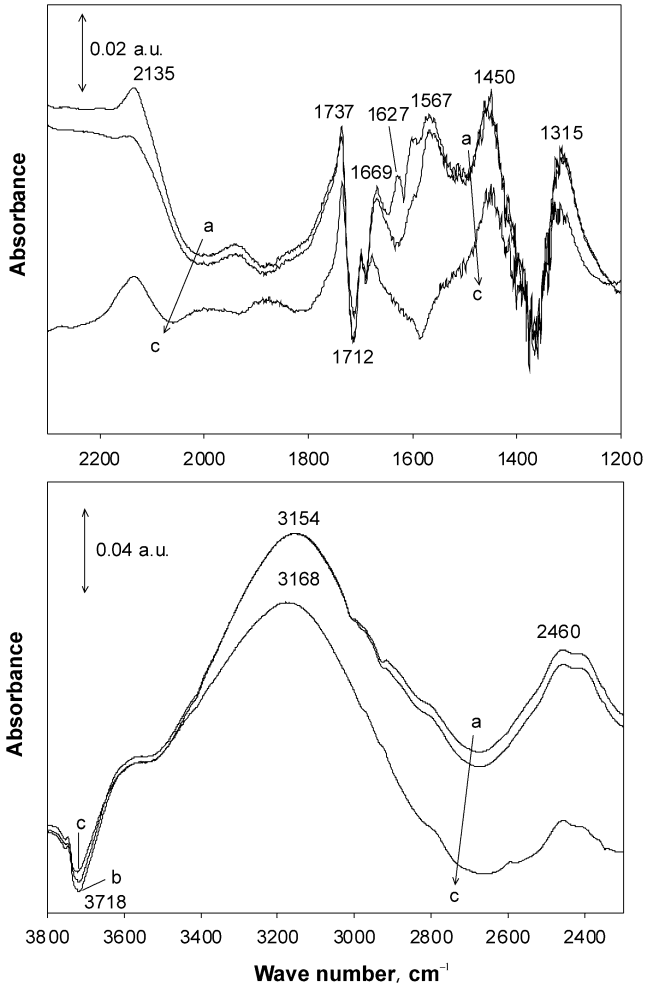

Fig. 8. Infrared spectroscopy spectra following NO_x treatment on Na-ZSM-5 at 30 °C in sequence: (a) 30 min NO_2 adsorption with 600 ppm NO_2, (b) 15 min 1st flushing with argon, (c) 15 min NO exposure.

zeolites following NO_x exposure. However, since the peak is very unstable upon argon flushing, it is more likely due to complexes of NO^+NO_2 or $NO^+N_2O_4$. These species might be formed following NO^+ formation in the presence of excess NO_2 [7,12].

Fig. 8 (spectra c) shows that introduction of 600 ppm NO to the sample following argon flushing results in an enormous change in the infrared spectra. The peaks at 1567 and 1669 cm^{-1} are almost completely removed by the NO introduction. At the same time, a collapse in intensity was observed in a wide wave number range of 3400–2000 cm^{-1}, which is in the hydrogen containing (X–H) stretching vibration region [27]. These observations might indicate a presence of nitric acid upon NO_2 adsorption. The peaks at 1567 and 1669 cm^{-1} are thus assigned to stretching vibrations of NO_2 of nitric acid molecules. Water present in the sample might cause the acid formation. It has been reported that even in thoroughly dried zeolite samples, traces of water remained that could lead to nitric acid formation [12]. An intensity decrease was observed at 1712 cm^{-1} during the NO_2 adsorption. However, the intensity of this peak then increased after the NO introduction. This band is thus assigned to the blue-shifted bending vibration of water molecules associated with zeolite frameworks. It was found that there was no significant change in infrared spectra with additional NO exposure.

As reported in some publications [12,13], in the presence of water NO_2 adsorption can take place through nitric acid formation

$$3NO_2 + H_2O \rightleftarrows 2HNO_3 + NO. \quad (1)$$

In addition, interaction between NO_2 and water molecules can also form HONO species [12]. The spectra band at 1315 cm^{-1} might represent NO_2^- from the HONO species. The formation of nitric acid during the NO_2 adsorption also contributes to the OH vibration appearance in the infrared spectra [12], as it appears in Fig. 8 as a broad peak in the range of 3600–2800 cm^{-1}.

Introduction of NO_2 to the sample at 30 °C also causes a band at 3718 cm^{-1} that decreases in intensity. This band is very close to the OH vibration of terminal hydroxyl groups in zeolites [19,22,23]. Argon flushing and NO exposure following the NO_2 saturation seem to recover this feature. This observation seems to indicate that the terminal OH groups can interact with NO_2-containing species [14].

Fig. 8 also shows another OH vibration evolution with a broad peak at around 3600 cm^{-1}. This peak might correspond to the formation of bridging hydroxyl groups [19,22,23]. It has been reported that in the presence of water, NO_2 adsorption on zeolites can form nitrates that accompany the formation of Brønsted acid sites [12,13,20]

$$HNO_3 + Zeo\text{–}O^-\text{–}Na^+ \rightleftarrows Na^+NO_3^- + Zeo\text{–}O^-\text{–}H^+. \quad (2)$$

According to this scheme, the peak at 1450 cm^{-1} might correspond to the stretching vibration of the nitrates associated with Na^+ [10]. The OH groups formed might contribute as a new site for further NO_2 adsorption [10,14,18]. This mechanism might explain the development of the broad peak of the bridging OH vibration spectra.

Fig. 9 shows that NO_2 adsorption at 200 °C results in slightly different infrared spectra. The peaks at 1567 and 1669 cm^{-1} are absent. Furthermore, the spectrum is much less intense in the high-wave-number region of 3400–2000 cm^{-1}. However, a broad spectrum still develops in the wave number range of 3700–3000 cm^{-1}, while another decreased in intensity at 1712 cm^{-1}. Furthermore, a peak with a band centered at about 3600 cm^{-1} is still observed. These observations seem to indicate that the NO_2 adsorption through nitric acid formation still occurs at 200 °C. In comparison with the adsorption at 30 °C, the intensity drop in the wave number range of 3400–2000 cm^{-1} from the adsorption at 200 °C might be due to the absence of NO_x-containing species weakly adsorbed on the sample. These species might be adsorbed on the sample through their interaction with nitric acid. It is suggested that NO_2 can bind to nitric acid through hydrogen bonding. This interaction magnifies the intensity of the spectra observed in the range

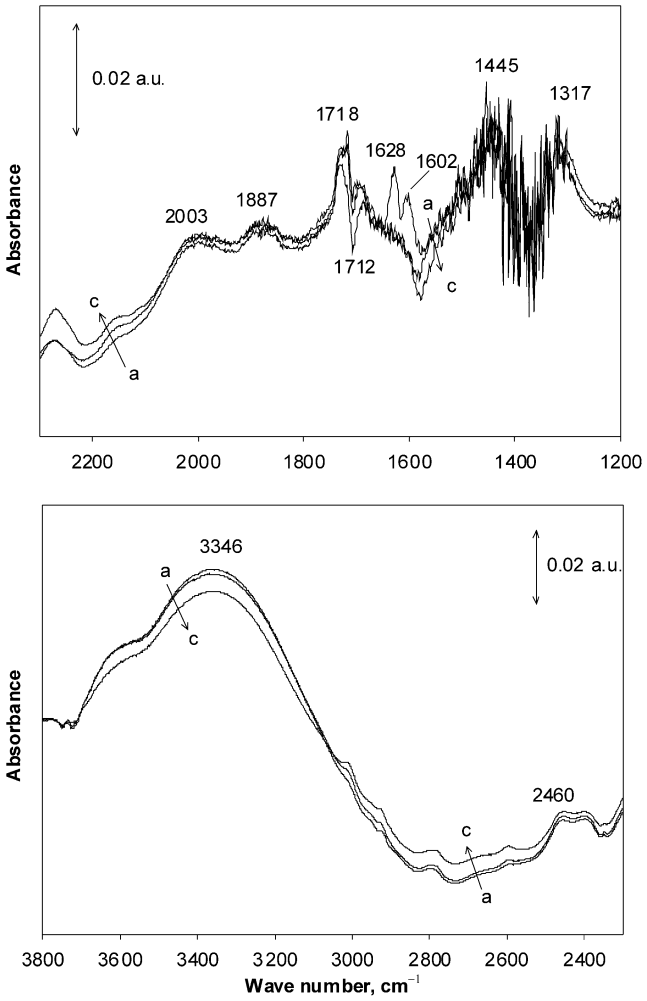

Fig. 9. Infrared spectroscopy spectra following NO_x treatment on Na-ZSM-5 at 200 °C in sequence: (a) 30 min NO_2 adsorption with 600 ppm NO_2, (b) 15 min 1st flushing with argon, (c) 15 min NO exposure.

of 3400–2000 cm^{-1}. As mentioned in the previous section, NO_2 adsorption over the monolith sample was accompanied by an almost constant NO production over the observed temperature range (see Fig. 4). This finding suggests that the amount of nitric acid formed in the zeolite framework according to reaction (1) is also rather constant with temperature. However, the nitric acid formed might contribute to the formation of weakly adsorbed NO_x. These species seem to have a slightly stronger bonding than physisorbed NO_2. This assertion is supported by the fact that a temperature increase carried out over the monolith sample following NO_2 equilibration at low temperature resulted in an immediate and large NO_x desorption (see Figs. 2 and 5). However, as mentioned previously, physisorbed NO_x remaining in the zeolite framework after flushing might also contribute to the desorption.

Infrared spectra generated from the adsorption at 200 °C as depicted in Fig. 9 indicates that the interactions between terminal OH and NO_x species seem to be absent from the adsorption. Fig. 9 shows that argon flushing following NO_2 saturation obviously removes peaks at 1602 and 1628 cm^{-1}, which previously were assigned to physisorbed NO_2. However, the flushing seems not to cause a significant change in the other peaks of the spectra.

Introduction of NO to the sample following argon flushing over the NO_2 equilibrated sample at 200 °C obviously reduces the intensity of the spectra in the OH vibration region. The NO exposure seems to be able to slightly recover the spectra in the wave number range of 3000–2000 cm^{-1}. At the same time the band at 1712 cm^{-1} regains its intensity. These observations suggest that the reversal of reactions (1) and (2) might take place during the NO exposure. However, it is difficult to observe intensity changes in the nitrate spectra bands because of noise in this region. It was found that there was no significant change in the intensity of the spectra with prolonged NO exposure.

NO_2 adsorption at 30 and 200 °C as shown in Figs. 8 and 9 also resulted in a development of a broad spectra band centered at 2460 cm^{-1}. This band corresponds to the vibration of zeolitic OH groups interacting with NO_x-containing species and is the B component of the A–B–C structure from hydrogen-bonded hydroxyls [10,19,22]. The A and C components at ∼2900 and ∼1700 cm^{-1}, respectively, are not clearly observed, since the peaks are obscured by high-intensity vibrations of other features. As shown in Figs. 8 and 9, these spectra are still clearly observed even after NO introduction. In addition to the presence of zeolitic OH groups due to the reaction (2), zeolitic OH groups present in the sample during sample preparation might also contribute to the evolution of these spectra. However, the broadness of the B band indicates the heterogeneity of hydroxyl sites in the ZSM-5 [26].

Fig. 10 shows infrared spectra from NO_2 adsorption at 350 °C. Features similar to those found at 200 °C were observed after introduction of 600 ppm NO_2 and argon flushing. However, it was observed that the species with spectra in the wave number range of 3700–3200 cm^{-1} were almost completely removed by NO introduction. Simultaneously, the spectra at lower frequencies (3200–2000 cm^{-1}) also recovered their intensities. The nitrate peak and another peak with a band at 2010 cm^{-1}, which is assigned to NO^+, are also affected and seem to decrease in intensity upon NO introduction. However, these two peaks are still present after a relatively long period of NO exposure. Given these observations, it can be asserted that another reaction scheme should be included to explain the presence of NO^+ and the nitrates species at 350 °C. It was reported [25,28] that NO_x can interact with Brønsted acid to form NO^+

$$2\text{Zeo–O}^-\text{–H}^+ + \text{NO}_2 + \text{NO} \rightleftarrows 2\text{Zeo–O}^-\text{–NO}^+ + \text{H}_2\text{O}. \quad (3)$$

Reaction (3), together with the reverse of reactions (1) and (2), is expected to occur during NO exposure over the NO_2-equilibrated sample. In addition, more stable nitrate species

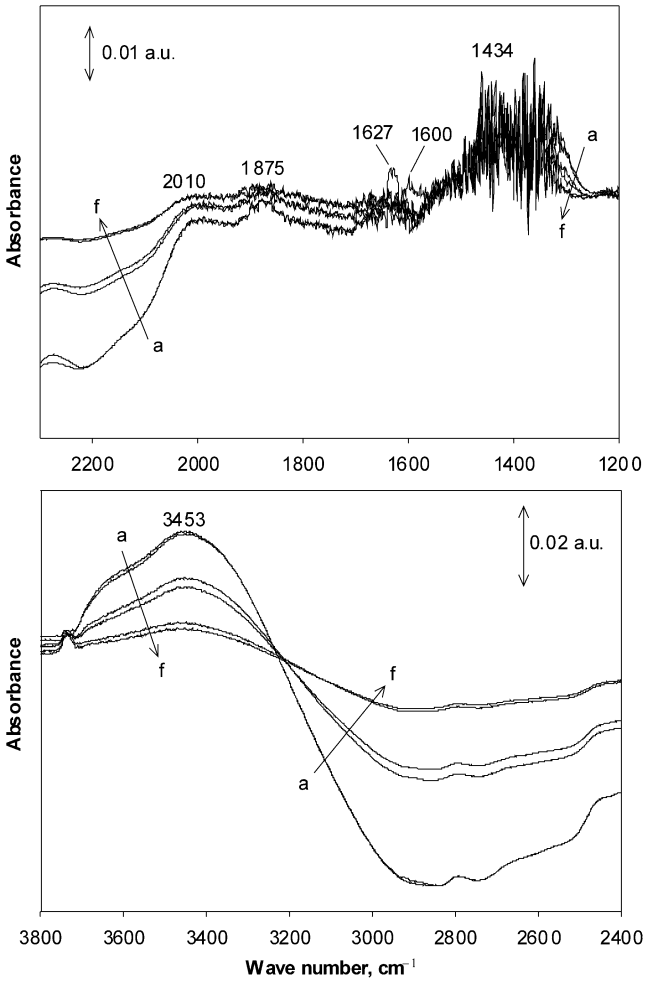

Fig. 10. Infrared spectroscopy spectra following NO_x treatment on Na-ZSM-5 at 350 °C in sequence: (a) 20 min NO_2 adsorption with 600 ppm NO_2, (b) 15 min 1st flushing with argon, (c) 15 min NO exposure, (d) 10 min 2nd flushing with argon, (e) 20 min NO re-exposure, (f) 10 min 3rd flushing with argon.

that are able to withstand NO exposure are probably formed through a disproportionation reaction of NO_2 [7,12,21]

$$2NO_2 \rightleftarrows N_2O_4, \tag{4}$$

$$N_2O_4 \rightleftarrows NO^+ + NO_3^-. \tag{5}$$

Subsequently the NO^+ binds to negatively charged sites in the zeolite framework, replacing the charge compensating Na^+, which is later bound to NO_3^-

$$\text{Zeo–O}^-\text{–Na}^+ + NO^+ + NO_3^- \rightleftarrows \text{Zeo–O}^-\text{–NO}^+ + Na^+NO_3^-. \tag{6}$$

Infrared spectra peaks with bands at 1737 and 1718 cm^{-1} from the NO_2 adsorption at 30 and 200 °C, respectively, indicate the presence of N_2O_4 [7,10,14,18,24]. However, the C band of the A–B–C structure might also interfere with this feature. At 350 °C this species was undetectable, suggesting that at high temperature a direct disproportionation of NO_2 might occur.

The infrared spectra generated from the NO_2 adsorption at 30, 200, and 350 °C are very useful for explaining the nature of the desorbed species during TPD. As observed from the experiments with the monolith samples, TPD following argon flushing over the NO_2 equilibrated monolith sample at 350 °C indicated the presence of two different nitrates. The nitrates can be distinguished by the introduction of NO (see Fig. 7). The nitrate reducible by NO is suggested to be formed via reactions (1) and (2). The other nitrate is more thermally stable, and NO is not involved in its formation. Instead, the formation follows a NO_2 disproportionation scheme via reactions (4) to (6). In addition to the nitrates, TPD after the adsorption at 200 °C results in medium thermally stable species (see Fig. 5). The infrared spectroscopy results indicate that these species correspond to NO_x-containing species interacting with Brønsted acids via hydrogen bonding. The interaction thus contributes to the OH vibration spectra. Furthermore, as the temperature increases a direct decomposition of nitric acid also contributes to the release of the moderately thermally stable species. Finally, NO_x-containing species bound to terminal hydroxyl groups, NO_x bound to nitric acid, NO_x with NO^+ as complexes of NO^+NO_2 or $NO^+N_2O_4$, and physisorbed NO_2 might contribute to the NO_x desorption below 200 °C.

3.4. Adsorption of a mixture of NO_2 and NO

The role of different nitrate species in NO_x adsorption at high temperature was further investigated. Before NO_2 adsorption, the sample was exposed to 400 ppm NO at 350 °C. It was observed that the NO concentration quickly increases, suggesting there is negligible adsorption of NO at this temperature. This assertion was supported by the fact that when the same step-change increase in NO was carried out with an empty reactor (without the monolith sample), the same NO concentration response was observed. Subsequently, NO_2 adsorption was carried out by the introduction of 600 ppm NO_2 in the 400 ppm NO present at constant temperature. As shown in Fig. 11a, an increase in NO concentration was observed immediately when the NO_2 was added. However, the amount of NO produced from NO_2 adsorption with the NO present is about two times less than the amount of NO produced without the simultaneous feed of NO (as in Fig. 3). This observation indicates that the nitrate formation through nitric acid that produces NO still occurs; however, it is impeded by the presence of NO. A competitive adsorption between NO and NO_2 would give a negligible contribution to the appearance of NO at this temperature. On the other hand, the amount of NO_2 adsorbed was unaffected by the feed of NO. TPD after equilibration and flushing gives a profile similar to that obtained from TPD after NO_2 equilibration followed by NO introduction and flushing (see Fig. 7b), except that the released NO_x concentrations are higher. These results certainly indicate that in the presence of NO, NO_2 storage involving NO formation is hindered. However, the fact that the amount of NO_2 adsorbed is not reduced and there

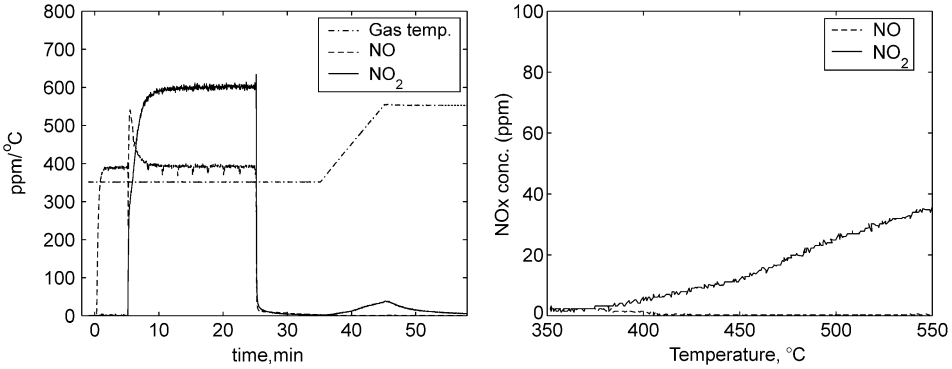

Fig. 11. Measured NO_x composition out of the reactor when sample was initially exposed to 400 ppm NO for 5 min and subsequently 600 ppm NO_2 for 20 min at a constant temperature 350 °C followed by a 10 min argon flush and finally a temperature ramp of 20 °C/min (a). NO_x concentration profiles during TPD after NO_x equilibration and argon flushing (b).

is mainly a greater desorption of the more thermally stable species in the TPD suggests that the presence of NO during adsorption in fact promotes the NO_2 adsorption through disproportionation of NO_2. These two adsorption mechanisms may be considered to compete for sodium cations on which to form nitrate species.

4. Conclusions

Depending on the temperature, NO_2 adsorption on ZMS-5-containing Na cations can result in various adsorbed species. There are three major types of adsorbed species present in the Na-ZSM-5 filmed sample. Physisorbed NO_2 and other weakly adsorbed NO_x species are present at temperatures up to about 150 °C. The quantity of these species was difficult to accurately quantify, because they may not have been removed completely by argon flushing, because of the high mass transport resistance in the zeolite film. In addition to hydroxyl groups, the presence of nitric acid in the adsorption contributes to the formation of both weakly and moderately thermally stable adsorbed species. Above 300 °C the adsorption predominantly results in nitrate species. There are two kinds of nitrates present from NO_2 adsorption. The nitrates can be formed either through nitric acid formation involving simultaneous NO production or the disproportionation reaction of NO_2, which forms more stable nitrate species. The presence of gas-phase NO serves to increase the formation of more stable nitrate species by the NO_2 disproportionation mechanism.

Acknowledgments

The authors are grateful for the financial support of the Swedish Research Council. I. Perdana and D. Creaser also thank the SIDA-Swedish Research Links program for support.

References

[1] M.A. Ulla, R. Mallada, J. Coronas, L. Gutierrez, E. Miró, J. Santamaria, Appl. Catal. B 253 (2003) 257.
[2] O. Öhrman, J. Hedlund, J. Sterte, Appl. Catal. A 270 (2004) 193.
[3] E.I. Basaldella, A. Kikot, C.E. Quincoces, M.G. Gonzalez, Mater. Lett. 51 (2001) 289.
[4] J. Hedlund, O. Öhrman, V. Msimang, E. van Steen, W. Bohringer, S. Sibya, K. Moller, Chem. Eng. Sci. 59 (2004) 2647.
[5] O. Öhrman, J. Hedlund, V. Msimang, K. Möller, Micropor. Mesopor. Mater. 78 (2005) 199.
[6] J. Despres, M. Koebel, O. Krocher, M. Elsener, A. Wokaun, Micropor. Mesopor. Mater. 58 (2003) 175.
[7] J. Szanyi, J.H. Kwak, R.A. Moline, C.H.F. Peden, Phys. Chem. Chem. Phys. 5 (2003) 4045.
[8] M. Katoh, T. Yamazaki, H. Kamijo, S. Ozawa, Zeolites 15 (1995) 591.
[9] E. Giamello, D. Murphy, G. Magnacca, C. Morterra, Y. Shioya, T. Nomura, M. Anpo, J. Catal. 136 (1992) 510.
[10] J. Szanyi, M.T. Paffett, J. Catal. 164 (1996) 232.
[11] K. Hadjiivanov, D. Klissurski, G. Busca, Appl. Catal. B 7 (1996) 251.
[12] J. Szanyi, J.H. Kwak, C.H.F. Peden, J. Phys. Chem. B 108 (2004) 3746.
[13] O. Monticelli, R. Loenders, P.A. Jacobs, J.A. Martens, Appl. Catal. B 21 (1999) 215.
[14] C. Sedlmair, B. Gil, K. Seshan, A. Jentys, J.A. Lercher, Phys. Chem. Chem. Phys. 5 (2003) 1897.
[15] J. Sterte, J. Hedlund, D. Creaser, O. Öhrman, W. Zheng, M. Lassinantti, Q. Li, F. Jareman, Catal. Today 69 (2001) 323.
[16] J. Sterte, J. Hedlund, B.J. Schoeman, US Patent 6,177,373 (2001), to Exxon Chemical.
[17] O. Öhrman, U. Nordgren, D. Creaser, J. Hedlund, J. Starte, in: A. Galarneau, F. Di Renzo, F. Fajula, J. Vedrine (Eds.), Zeolites and Mesoporous Material at the Dawn of the 21st Century, Studies in Surface Science and Catalysis, vol. 135, Elsevier, Amsterdam, 2001, p. 20-P-09.
[18] K.I. Hadjiivanov, Catal. Rev.-Sci. Eng. 42 (2000) 71.
[19] J. Sárkány, Appl. Catal. A 118 (1999) 369.
[20] A. Sultana, R. Loenders, Monticelli, C. Kirschhock, P.A. Jacobs, J.A. Martens, Angew. Chem. Int. Ed. 39 (2000) 2934.
[21] E. Ito, Y.J. Mergler, B.E. Nieuwenhuys, H. van Bekkum, C.M. van den Beek, Micropor. Mesopor. Mater. 4 (1995) 455.
[22] K. Hadjiivanov, J. Saussey, J.L. Freysz, J.C. Lavalley, Catal. Lett. 52 (1998) 103.

[23] A. Dryer, An Introduction to Zeolite Molecular Sieves, John Willey and Sons, New York, 1988, p. 122.
[24] K. Hadjiivanov, Micropor. Mesopor. Mater. 24 (1998) 41.
[25] A. Penkova, K. Hadjiivanov, Catal. Commun. 4 (2003) 485.
[26] J. Datka, M. Boczar, B. Gill, Langmuir 9 (1992) 2496.
[27] J.W. Niemantsverdriet, Spectroscopy in Catalysis: An Introduction, Willey, New York, 2000.
[28] M. Mihaylov, K. Hadjiivanov, D. Panayotov, Appl. Catal. B 51 (2004) 33.